BIOCHEMISTRY
including biophysical chemistry & molecular biology
Article

Biochemistry **2010,** *49,* 951–957 951
DOI: 10.1021/bi9017335

Distal Interactions within the par3−VE-Cadherin Complex[†,‡]

Robert C. Tyler, Francis C. Peterson, and Brian F. Volkman*

Department of Biochemistry, Medical College of Wisconsin, Milwaukee, Wisconsin 53226

Received October 7, 2009; Revised Manuscript Received January 4, 2010

ABSTRACT: par3 is a multiple-PDZ-containing scaffold protein that is central to the organization of an evolutionarily conserved cell polarity complex consisting of par3, par6, and aPKC. The ability of par3 PDZ domains to target various adhesion molecules and enzymes at the plasma membrane leads to the controlled localization of par6 and aPKC, which has firmly established its role in epithelial cell polarity. Of the numerous PDZ ligands associated with par3, interaction of its third PDZ domain with the class II ligand found within the C-terminal tail of vascular endothelial cadherin (VE-Cad) suggests a role in endothelial cell polarity as well, but the molecular details of the interaction are unknown. Previously determined structures of par3-PDZ3 bound to the class I ligand found within the C-terminal tail of the phosphoinositide phosphatase PTEN revealed two discrete binding sites: a canonical PDZ−ligand interaction site and a distal site involving charge−charge complements. Currently, it is unclear if par3-PDZ3 employs both canonical and distal binding modes in its association with VE-Cad or if these modes are unique to the PTEN interaction, suggesting a possible mechanism for ligand specificity within the polarity network. The structure of par3-PDZ3 bound to the C-terminal tail of VE-Cad presented in this work shows that both canonical and distal interactions are utilized in binding. Biophysical measurements using fluorescence polarization and two-dimensional NMR implicate the intermolecular charge pairing of aspartic acid 777 (VE-Cad) and arginine 609 (par3-PDZ3) as a crucial modulator of complex formation. Phosphorylation of VE-Cad at serine 776 increases its affinity for par3, demonstrating that post-translational modifications outside of the canonical carboxylate binding site can enhance PDZ−ligand interactions. Comparison of the VE-Cad and PTEN complexes highlights how the unique molecular architecture of par3-PDZ3 can accommodate both canonical and distal interaction modes that allow dual-class specificity for these two ligand types.

The formation and disassembly of large protein complexes are critically important in the regulation of cellular communication. Elucidating the molecular determinants that govern protein−protein interactions greatly enhances our understanding and ability to manipulate signaling pathways in the treatment of disease. Of the ~150 families of protein interaction domains (*1*), the PDZ[1] domain is one of the most abundant and best characterized (*2*). PDZ domains derive their name from the first three proteins in which the domain was discovered (PSD-95, Disc large, and ZO-1) (*3*). The domain consists of ~90 amino acids that fold into a six-stranded β-sheet capped by two α-helices. Typically, PDZ domains bind to extreme carboxyl-terminal (C-terminal) peptide ligands found within particular protein targets but are capable of a diverse range of ligand interactions. For instance, PDZ domains can also bind internal protein sequences (*4*, *5*), as well as phosphoinositides (PIPs) (*6*). These unique properties allow PDZ domains to participate in a wide range of interactions that often result in localization of specific protein complexes within the cellular membrane (*7*).

C-Terminal peptide binding is the most characterized mode of PDZ domain interaction. In this case, peptide binding is facilitated by a structurally conserved groove formed between strand β2 and helix α2 of the PDZ domain (*8*). Canonical peptide binding occurs at the P_0 and P_{-2} positions that form amide hydrogen bonds that anchor into the PDZ binding groove (P_0 denotes the C-terminal residue of the peptide ligand, and P_{-n} denotes the *n*th amino acid from the C-terminus). As a result, C-terminal target peptides are organized into classes depending on the composition of residues at the P_0 and P_{-2} positions. Class I, II, and III peptide ligands are comprised of the -(S/T)-X-Φ_{COO-}, -Φ-X-Φ_{COO-}, and -G-(E/D)-X-Φ_{COO-} motifs, respectively, with single letters representing amino acids, X any amino acid, and Φ any hydrophobic amino acid (*9*). Of the numerous peptide ligands that have been identified as PDZ binders, most contain hydrophobic residues at the C-terminal position. However, in contrast to the groupings described above, class IV ligands are identified by the -X-Φ-D/E_{COO-} motif that contains a negatively charged side chain at P_0. Whereas most PDZ domains are thought to associate with a single class of ligand, examples of PDZ domains with dual-class specificity have been reported (*10*−*12*).

Although positions P_0 and P_{-2} form strong contacts with the PDZ domain, other residues further upstream can also contribute to ligand binding. An earlier study indicated that residues up to P_{-8} could affect the ligand specificity of discs large PDZ3 (*13*). Distal binding interactions have also been observed in PDZ domains from the human phosphatase hPTP1E (*14*) and erbin (*15*), where respective ligand positions P_{-6} and P_{-7} can

[†]This work was supported by National Institutes of Health (NIH) Protein Structure Initiative Grant U54 GM074901 [J. L. Markley (principal investigator), G. N. Phillips, and B. G. Fox (co-investigators)] and NIH Instrumentation Grant S10 RR024665.

[‡]The structure of the PDZ3−VE-Cad complex has been deposited in the Protein Data Bank as entry 2KOH. All NMR data have been deposited in the BMRB under accession number 16507.

*To whom correspondence should be addressed. E-mail: bvolkman@mcw.edu. Phone: (414) 955-8400. Fax: (414) 456-6510.

[1]Abbreviations: FP, fluorescence polarization; par3, partition defective protein 3; PDZ, PSD-95, Disc large, and ZO-1; VE-Cad, vascular endothelial cadherin; PDB, Protein Data Bank.

Published on Web 01/04/2010

interact with an extended loop between strands β2 and β3 of the PDZ domain.

Partition defective protein 3 (par3) is a large scaffold protein containing three PDZ domains (PDZ1−3) that interact with multiple target proteins. It was first demonstrated that par3-PDZ1 associated with C-terminal ligands found within junction adhesion molecules (JAMs), which led to speculation about its role in epithelial and endothelial cell polarity (*17*). Subsequent studies revealed that PDZ1 also binds the C-terminal tail of nectin (*18*), another adhesion molecule, as well as phospholipase C-β (*19*). Permissive binding has been demonstrated for par3-PDZ2, which has been shown to associate with certain PIPs within lipid membranes (*20*). This interaction involves residues from the α2−β6 and β1−β2 loops and appears to be critical for epithelial cell polarity. Investigations of par3-PDZ3 have shown affinities toward C-terminal ligands found in JAM-C (*21*), vascular endothelial cadherin (VE-Cad) (*22*), and the PIP phosphatase PTEN (*16*). Given that par3 interacts with both PIPs and PTEN, it is now believed that par3 plays a major role in the integration of PIP signaling events during epithelial cell polarization (*16*).

Structural investigation of the par3-PDZ3−PTEN complex has revealed canonical PDZ interactions involving P_0 and P_{-2}, as well as distal interactions that reach the P_{-10} register of the target peptide (*16*). These distal contacts result, in part, from distinctive structural aspects of the PDZ domain. Relative to other PDZ domains, par3-PDZ3 possesses a slightly longer α2 helix, resulting in an elongated ligand binding groove. This feature creates additional surface area facilitating complementary side chain interactions involving acidic residues D^{393}, E^{394}, and D^{395} (i.e., P_{-8}, P_{-9}, and P_{-10}, respectively) of PTEN and basic residues (K^{606}, R^{609}, K^{611}, and K^{622}) within the extended β2 and β3 regions of par3-PDZ3 (*16*). Interestingly, PTEN is recognized as a class I C-terminal ligand containing the -T-K-V_{COO-} motif, while both JAM-C and VE-Cad contain putative class II ligands -F-V-I_{COO-} and L-I-I_{COO-} at their respective C-termini. Given the dual specificity of par3-PDZ3 for C-terminal ligands, we investigated the degree to which the reported noncanonical distal interactions contribute to its affinity for different binding partners.

Here we report the NMR structure of par3-PDZ3 in complex with the C-terminal tail of VE-Cad. Canonical interactions in the carboxylate binding pocket are augmented by an association between distal parts of the peptide and the extended β2 region of the PDZ domain. Using fluorescence polarization to measure peptide binding affinity and two-dimensional (2D) NMR to monitor specific interactions, we show that D^{777} (P_{-7}) of VE-Cad and R^{609} of par3-PDZ3 make significant contributions to binding. Interestingly, phosphorylation of VE-Cad at P_{-8} (S^{776}) also enhances PDZ3 binding.

EXPERIMENTAL PROCEDURES

Protein Expression, Purification, and Mutagenesis. The amino acid sequence of par3-PDZ3 (residues 581−689) was PCR amplified from *Mus musculus* par3 and cloned into a modified pQE30 vector (Qiagen) containing a cleavable N-terminal His_8 tag. Protein was expressed in SG13009 *Escherichia coli* cells and purified by Ni^{2+} affinity chromatography. The resulting protein was cleaved with TEV protease to remove the His_8 affinity tag and further purified by cation exchange chromatography. Unlabeled protein was prepared from growth in Luria-Bertani medium. Uniformly labeled ^{15}N-labeled or ^{15}N- and ^{13}C-labeled proteins used in NMR experiments were prepared from growth in M9 minimal medium incorporating [U-^{13}C]glucose [Cambridge Isotope Laboratories (CIL)] and/or [U-^{15}N]-ammonium chloride (CIL) as the sole carbon or nitrogen sources. A cDNA fragment encoding the 16 C-terminal residues of *M. musculus* VE-Cad was also cloned into a modified pQE30 vector containing a cleavable N-terminal His_8-GB1 tag. The uniformly labeled [^{15}N,^{13}C]VE-Cad peptide was expressed in SG13009 *E. coli* cells from growth in M9 minimal medium incorporating [U-^{13}C]glucose (CIL) and [U-^{15}N]ammonium chloride (CIL) as the sole carbon and nitrogen sources, respectively, and purified by Ni^{2+} affinity chromatography. After removal of the His_8-GB1 tag, the peptide was further purified by reverse-phase HPLC using a 10 to 70% acetonitrile gradient, followed by lyophilization. The identity and molecular mass of ^{15}N- and ^{13}C-labeled peptide were verified by matrix-assisted laser desorption ionization mass spectrometry (MALDI-MS) and NMR (Figure S1 of the Supporting Information). To create the alanine-substituted par3-PDZ3 R609A protein, site-directed mutagenesis was performed using pairs of complementary primers and the QuickChange kit (Stratagene) following the manufacturer's protocol.

Peptide Synthesis. The Protein Nucleic Acid Facility (PNA) at the Medical College of Wisconsin synthesized all unlabeled and rhodamine-labeled VE-Cad peptides with rhodamine coupled to the N-terminus using standard Fmoc chemistry.

NMR Spectroscopy. NMR experiments were performed on a Bruker DRX 600 instrument equipped with a ^1H, ^{15}N, ^{13}C cyroprobe. NMR titration experiments were performed with 100 μM ^{15}N-labeled par3-PDZ3 in 20 mM sodium phosphate, 50 mM NaCl, and 3 mM dithiothreitol (DTT) (pH 6) at 298 K. Complete resonance assignment were achieved for 1 mM ^{15}N- and ^{13}C-labeled par3-PDZ3 saturated with (2 mM) unlabeled VE-Cad peptide (MLAELYGSDPQEELII$_{COO-}$) using the following experiments: 2D $^{15}N-^1H$ HSQC, three-dimensional (3D) HNCA, 3D HNCO, 3D HNCACB, 3D HNCACO, 3D HN(CO)CA, 3D C(CO)NH, 3D HBHACONH, 3D HC(CO)NH, and 3D HCCH-TOCSY. Complete resonance assignments were achieved for 1 mM ^{15}N- and ^{13}C-labeled VE-Cad peptide (MLAELYGSDPQEELII$_{COO-}$) saturated with 1 mM par3-PDZ3 in 20 mM sodium phosphate, 50 mM NaCl, and 3 mM dithiothreitol (pH 6) at 298 K with the following experiments: 2D $^{15}N-^1H$ HSQC, 3D HNCA, 3D HNCO, 3D HNCACB, 3D C(CO)NH, 3D HC(CO)NH, and 3D HCCH-TOCSY. All NMR data were processed with NMRPipe (*23*), and XEASY (*24*) was used for resonance assignment and analysis of NOE spectra.

Structure Calculation and Analysis. NOE distance restraints were obtained from 3D ^{15}N-edited NOESY-HSQC, ^{13}C(aliphatic)-edited NOESY-HSQC, ^{13}C(aromatic)-edited NOESY-HSQC, and $^{13}C-^{12}C$-filtered NOESY-HSQC (*25*) spectra (τ_{mix} = 80 ms). Backbone dihedral angle restraints (ϕ and ψ angles) were derived from $^1H^\alpha$, $^{13}C^\alpha$, $^{13}C^\beta$, $^{13}C'$, and ^{15}N chemical shift data using TALOS (*26*). Structures were generated in an automated manner using the NOEASSIGN module of the torsion angle dynamics program CYANA version 2.1 (*27*). This procedure resulted in an ensemble of high-precision structures that required minimal manual refinement. The 20 CYANA conformers with the lowest target function were further refined by a molecular dynamics protocol in explicit solvent (*28*) using XPLOR-NIH (*29*).

Fluorescence Polarization Assay. The fluorescence polarization (FP) assays were performed on a PTI (Photon Technologies International) fluorimeter equipped with automated polarizers at 298 K. Synthetic VE-Cad peptides were labeled with rhodamine at the N-terminus. Titrations were conducted by monitoring fluorescence polarization as a function of increasing amounts of par3-PDZ3 added to 100 nM rhodamine-VE-Cad peptide in 50 mM HEPES, 100 mM NaCl, 1 mM DTT, and 1 mM EDTA (pH 7.4), using excitation and emission wavelengths of 562 and 582 nm, respectively. The dissociation constants (K_d) were determined by fitting titration curves using profit 6.1 to the equation

$$FP_{obs} = FP_o + \frac{x(FP_{max} - FP_o)}{K_d + x}$$

where FP_{obs} is the observed FP value, FP_o is the value of the free peptide, FP_{max} is maximum value of the completely bound peptide, and x is the par3-PDZ3 protein concentration.

RESULTS AND DISCUSSION

Identification of the VE-Cadherin Binding Site on par3-PDZ3. The association of VE-Cad with par3 in endothelial cells is mediated by PDZ3 of par3 and the VE-Cad C-terminus (*22*). To detail the structural basis for this important polarity complex, we identified the VE-Cad binding site of par3-PDZ3 using $^1H-^{15}N$ HSQC NMR spectroscopy. In these experiments, ^{15}N-labeled par3-PDZ3 was titrated with a synthetic peptide comprising the last 16 amino acids of VE-Cad shown in Figure 1A. Chemical shift perturbations caused by the addition of VE-Cad were mapped onto the 3D structure of the ligand free form of par3-PDZ3 [PDB entry 2K1Z (*16*)] shown in Figure 1B. Consistent with C-terminal peptide binding, residues within the $\beta2-\alpha2$ binding groove (e.g., G^{600}, L^{601}, G^{602}, and V^{605}) displayed the most prominent chemical shift perturbations upon addition of VE-Cad. We also observed marked peptide-induced chemical shift perturbations for a cluster of basic residues, including K^{606}, R^{609}, K^{611}, and K^{622}, all of which extend beyond the $\beta2-\alpha2$ binding groove. We speculated that conserved acidic amino acids near the VE-Cad C-terminus (Figure 1A) might interact with the basic patch of par3-PDZ3.

Structure of par3-PDZ3 in Complex with the C-Terminus of VE-Cad. To define the nature of the par3-PDZ3−VE-Cad interaction, the structure of par3-PDZ3 in complex with the VE-Cad peptide was determined by NMR. Initially, ^{15}N- and ^{13}C-labeled par3-PDZ3 was titrated with unlabeled VE-Cad (Figure 1A) until saturation was reached. Standard heteronuclear NOESY spectra (i.e., ^{15}N-edited and ^{13}C-edited) were processed and analyzed for use in automated NOE assignment. Intermolecuar NOEs between the labeled PDZ domain and the unlabeled peptide were also obtained from $^{13}C-^{12}C$-filtered NOESY spectra. Conversely, a complex of ^{15}N- and ^{13}C-labeled VE-Cad peptide with unlabeled par3-PDZ3 was used for acquisition of a complete set of heteronuclear and $^{13}C-^{12}C$-filtered spectra. After final analysis, 1868 NOE distance restraints were used in calculation of an ensemble of structures representing the par3-PDZ3−VE-Cad complex.

The final ensemble of par3-PDZ3 in complex with the VE-Cad peptide is displayed in Figure 2A, with structural statistics listed in Table 1. Comparison of our PDZ domain complex to the reported ligand free form (PDB entry 2K1Z) revealed a

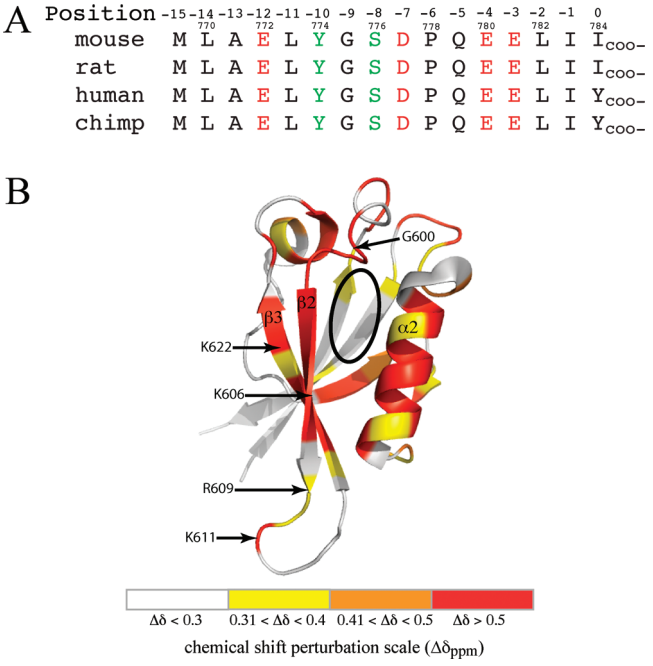

FIGURE 1: (A) Sequence alignment of the 16 terminal amino acids of VE-Cad. Position indicates the register of amino acids relative to the C-terminus denoted as 0. The mouse (*M. musculus*) sequence shown corresponds to the exact peptide used in NMR titration studies, with numbers above corresponding to amino acid locations in the primary sequence. Conserved acidic residues are colored red, and potential phosphorylation sites are colored green. (B) Chemical shift perturbations induced by VE-Cad peptide binding mapped onto the structure of ligand free par3-PDZ3. Differences in amide chemical shifts were defined by the relationship $\Delta\delta_{ppm} = [(5\Delta\delta_{HN})^2 + (\Delta\delta_N)^2]^{1/2}$, where $\Delta\delta_{HN}$ and $\Delta\delta_N$ represent chemical shift differences of the free and bound forms of par3-PDZ3, respectively. The black oval highlights the location of the binding groove between strand $\beta2$ and helix $\alpha2$, the site of canonical C-terminal ligand binding. Positions of basic patch residues (K^{606}, R^{609}, K^{611}, and K^{622}) located in strands $\beta2$ and $\beta3$ are shown to distinguish areas of distal ligand binding.

C^α backbone alignment root-mean-square deviation (rmsd) of 1.59 Å. The geometries of the two PDZ domains are in excellent agreement, with the only difference seen in the orientation of the $\alpha2$ helix resulting from an outward rotation caused by entry of a ligand into the binding groove. This same helical rotation has been reported in the par3-PDZ3−PTEN complex (*16*). Consistent with C-terminal peptide binding, P_0 of VE-Cad (I^{784}) packs into a cavity created by residues L^{601} and V^{603} of the conserved "GLGF" motif between strands $\beta1$ and $\beta2$, and M^{666} in helix $\alpha2$ shown in panels B and C of Figure 2. Additional hydrophobic side chain contacts are observed between P_{-1} (I^{783}) and I^{625}, as well as P_{-2} (L^{782}) and M^{659} located in helix $\alpha2$ (Figure 2C). The VE-Cad peptide contains four acidic residues at P_{-3} (E^{781}), P_{-4} (E^{780}), P_{-7} (D^{777}), and P_{-12} (E^{772}) that could potentially serve as interaction partners with the distal basic patch unique to par3-PDZ3. NOEs between P_{-3} (E^{781}) and K^{606} confirmed the pairing of these residues, and the side chain orientation of K^{622} places the positively charged headgroup in the proximity of the glutamate side chain of P_{-3} (E^{781}), well within hydrogen bonding distance. This configuration suggested that movements of amide cross-peaks K^{606} and K^{622} observed in $^1H-^{15}N$ HSQC titration experiments are likely caused by interactions with E^{781} of VE-Cad. NOE contacts between P_{-4} (E^{780}) and N^{655} located at the N-terminal end of helix $\alpha2$ were observed, resulting in the glutamate side chain pointing away from strand $\beta2$. Interestingly,

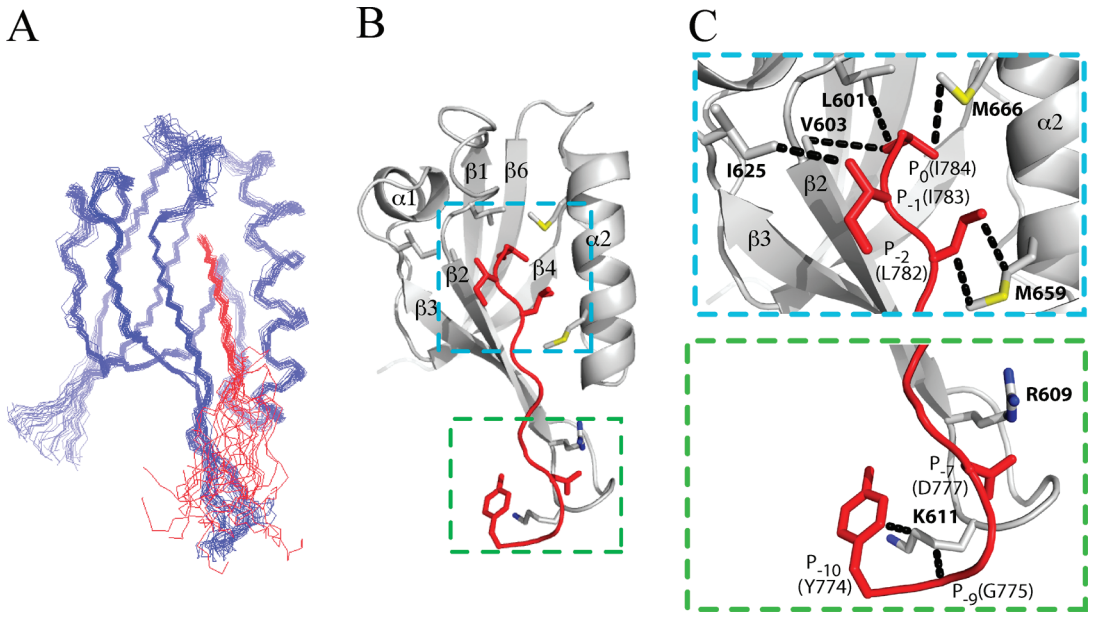

FIGURE 2: (A) Solution structure of par3-PDZ3 in complex with the VE-Cad peptide. An overlay of 20 conformers with the VE-Cad peptide is colored red, where the unstructured N- and C-termini have been deleted for the sake of clarity. (B) Ribbon diagram of the representative conformer showing areas of secondary structure. The cyan box highlights the region of canonical interaction, and the green box highlights the region of distal interactions. (C) Zoomed-in view of the canonical (top) and distal (bottom) binding sites. Dashed lines between molecules represent areas of observed NOEs described in text. Bold numbering indicates amino acids within par3-PDZ3, and P_n terms represent amino acid positions within the peptide.

several structures in the ensemble place the acidic side chain of P_{-7} (D^{777}) in the proximity of the guanidinium group of R^{609} (Figure 2C), though no intermolecular NOEs were detected for this pair of residues. In contrast, P_{-12} (E^{772}) is disordered and does not appear to contact par3-PDZ3. Weak NOEs from both the P_{-9} (G^{775}) and P_{-10} (Y^{774}) residue to K^{611} within the $\beta2-\beta3$ turn of par3-PDZ3 define the most distal interaction with the extended binding groove (Figure 2C). A schematic diagram representing all amino acid residues involved in intermolecular binding observed within the par3-PDZ3−VE-Cad complex is shown in Figure S2 of the Supporting Information.

Table 1: Structural Statistics for the 20 par3-PDZ3−VE-Cad Conformers

experimental constraints	PDB entry 2KOH
no. of distance constraints	
long	735
medium ($1 < i - j \leq 5$)	254
sequential ($i - j = 1$)	383
intraresidue ($i = j$)	434
inter-residue	62
total	1868
dihedral angle constraints (ϕ and ψ)	114
average atomic rmsd from the mean structure (Å) for residues 8−16, 22−30, and 38−103	
backbone (C^{α}, C′, N)	0.44 ± 0.07
heavy atoms	0.93 ± 0.09
deviations from idealized covalent geometry	
rmsd for bond lengths (Å)	0.019
rmsd for torsion angle violations (deg)	1.4
WHATCHECK quality indicators	
Z score	−1.30 ± 0.20
rms *Z* score	
bond lengths	0.88 ± 0.02
bond angles	0.71 ± 0.02
bumps	0 ± 0
Lennard-Jones energy[a] (kJ/mol)	−2408 ± 51
constraint violations	
no. of NOE distances >0.5 Å	0 ± 0
rmsd for NOE distances (Å)	0.023 ± 0.001
no. of torsion angle violations >5°	0 ± 0
rmsd for torsion angle violations (deg)	0.674 ± 0.097
Ramachandran statistics (% of all residues)	
most favored	81.6 ± 3.2
additionally allowed	16.5 ± 3.0
generously allowed	1.1 ± 1.0
disallowed	0.7 ± 0.8

[a]The nonbonded energy was calculated in XPLOR-NIH.

VE-Cadherin Composition Has an Effect on par3-PDZ3 Binding. Our structural analysis indicated that in addition to the canonical P_0 and P_{-2} binding sites, amino acids as distant from the VE-Cad C-terminus as P_{-10} contributed to par3-PDZ3 recognition. On the basis of the contacts between P_{-10} (Y^{774}) and K^{611}, we speculated that P_{-7} (D^{777}) of VE-Cad might interact with R^{609} of par3. To probe specific contributions of distal contacts to the par3-PDZ3−VE-Cad interaction, we determined binding constants (K_d) for several different VE-Cad constructs using fluorescence polarization. If the P_{-10} and P_{-7} positions enhance the interaction with par3-PDZ3, there should be a measurable difference in binding affinities between C-terminal constructs lacking these residues. Rhodamine-labeled peptides containing either the six or twelve C-terminal residues of VE-Cad were used to measure par3-PDZ3 binding constants by FP (Figure 3A). VE-Cad(773−784) bound PDZ3 ~5-fold more tightly than VE-Cad(779−784), indicating that residues in the $P_{-11}-P_{-6}$ register contribute ~1 kcal/mol to the free energy of binding. Guided by the par3-PDZ3−VE-Cad structure, we measured binding affinities for VE-Cad(773−784) peptides containing a Y774A or D777A mutation (Figure 3B). While the Y774A substitution has a modest effect on K_d, the D777A mutation at P_{-7} shifts the K_d from 6 ± 2 to 42 ± 10 μM, comparable to that of the six-residue peptide (28 ± 8 μM). This suggests that the P_{-7} residue of VE-Cad (D^{777}) is the major contributor to distal binding.

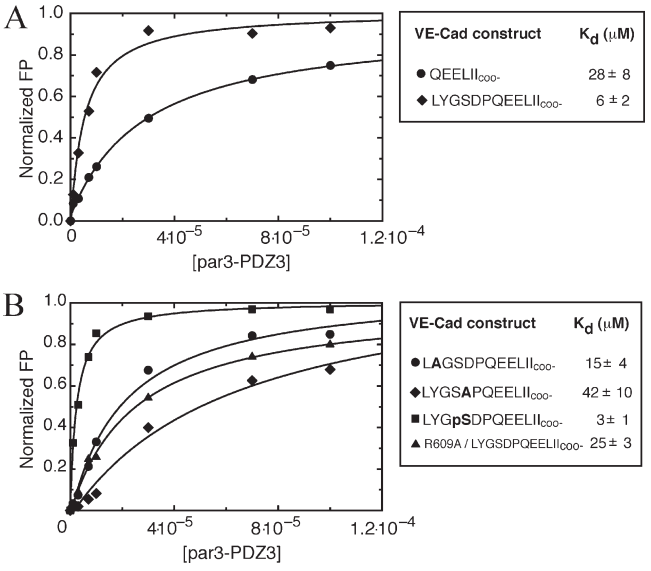

FIGURE 3: (A) Determination of affinity for different length VE-Cad peptides binding to par3-PDZ3 using a fluorescence polarization assay. All peptides contained the N-terminally linked rhodamine label. Comparison of binding curves of short (●) and long (◆) constructs of VE-Cad revealed a ~5-fold increase in binding affinity for the longer VE-Cad segment. (B) Comparison of binding curves generated for YtoA (●) and DtoA (◆) VE-Cad mutants revealed that P_{-7} (D) contributes to the interaction of VE-Cad with par3-PDZ3 as indicated by the decrease in binding affinity. The R609A mutation of par3-PDZ3 (▲) shows a decrease in binding affinity when titrated against the long VE-Cad construct. Further modification of VE-Cad by phosphorylation of P_{-8} (S) (■) revealed that additional negative charge introduced into distal amino acids can increase the level of binding relative to the long construct by ~2-fold. Bold letters signify the location of alanine substitutions or serine phosphorylation (pS). The error in K_d is estimated from fitting.

Mutation of R^{609} of par3-PDZ3 Reduces the VE-Cad Binding Affinity. To further test for the presence of a distal interaction between R^{609} and D^{777} in the par3-PDZ3−VE-Cad complex, we constructed a par3-PDZ3 protein containing a R609A mutation. We speculated that the R609A mutation should disrupt charge pairing with D^{777} in wild-type VE-Cad, resulting in a measurable decrease in binding affinity. The R609A mutant revealed a VE-Cad binding K_d of 25 ± 3 μM (Figure 3B), reinforcing our hypothesis that a $D^{777}-R^{609}$ intermolecular salt bridge is the major contributor to distal binding in the par3-PDZ3−VE-Cad complex.

Possible Role of Serine Phosphorylation in the VE-Cad C-Terminus. Having recognized the importance of side chain-mediated contacts governing the par3-PDZ3−VE-Cad complex, we next determined if post-translational modifications could further increase binding affinity by introducing additional complementary charges. VE-Cad contains two potential phosphorylation sites at P_{-10} (Y^{774}) and P_{-7} (S^{776}) that could interact with basic residues of par3-PDZ3, and S^{776} is predicted to be a target for casein kinase 2 (*30*). Both phosphopeptides were synthesized and titrated against ^{15}N-labeled par3-PDZ3. Screening by $^{1}H-^{15}N$ HSQC revealed binding affinities of ~2 and ~6 μM for the pS^{776}- and pY^{774}-containing VE-Cad peptides, respectively. Since the wild-type VE-Cad peptide (residues 773−784) binds par3-PDZ3 with a binding affinity of 6 μM, these results suggested that phosphorylation of S^{776} but not Y^{774} enhances par3-PDZ3 binding, and we confirmed the increased binding affinity by FP (Figure 3B). This suggests that specific serine phosphorylation within the VE-Cad C-terminus creates an additional electrostatic interaction with basic residues of par3-PDZ3.

The D777A VE-Cadherin Mutant Has an Effect on Distal par3-PDZ3 Interactions. If a stable $D^{777}-R^{609}$ salt bridge is critical in the formation of the par3-PDZ3−VE-Cad complex, it seems NOEs would be detected. However, if the side chains of D^{777} and R^{609} point toward each other, the shortest interproton distance (from H^{ε} of R^{609} to the H^{β} protons of D^{777}) would be ~6 Å. Hence, the lack of observable NOEs between R^{609} and D^{777} is not inconsistent with a side chain-mediated electrostatic interaction. To confirm the function of D^{777} in side chain-mediated binding, the alanine-substituted peptide was titrated against ^{15}N-labeled par3-PDZ3 to detect site-specific perturbations to backbone amide resonances. We hypothesized that if the D777A-VE-Cad mutant disrupted side chain-mediated binding, differences in backbone amide resonances along strand β2 of par3-PDZ3 should be evident when compared to a wild-type VE-Cad titration spectrum. Comparisons of the $^{1}H-^{15}N$ HSQC spectra of ^{15}N-labeled par3-PDZ3 saturated with either D777A-VE-Cad (red) or wild-type VE-Cad (gray) show that while most cross-peaks are in identical positions ($\Delta\delta_{ppm} < 0.09$), several residues (e.g., K^{606}, G^{607}, N^{608}, and R^{609}) display differences in resonance position (Figure 4). Identical experiments performed with the Y774A-VE-Cad peptide showed no differences attributable to the substitution (data not shown). These results confirm that D^{777} is the major contributor of distal VE-Cad contacts to par3-PDZ3 and likely serves as an anchor to upstream regions of the peptide that allows further interaction along extended strand β2 of par3-PDZ3.

par3-PDZ3 Complexes Reveal the Source of Dual Ligand Class Specificity. par3-PDZ3 employs two distinct binding modes in the interaction with the class II ligand found within the C-terminal tail of VE-Cad, similar to interactions reported for the class I C-terminal PTEN ligand (*16*). Both ligands exploit the hydrophobic cavity formed by residues L^{601}, V^{603}, and M^{666} on par3-PDZ3, and both ligands use additional distal contacts to further stabilize binding (Figure 5). However, there are subtle differences that may explain the molecular basis of dual specificity that par3-PDZ3 displays toward these two ligand classes. One key factor is the absence of a conserved histidine within helix α2 of par3-PDZ3 that is associated with the recognition of class I PDZ ligands. Typically, this histidine residue forms a hydrogen bond with the hydroxyl group of the serine or theronine at P_{-2} of class I ligands (*31*). par3-PDZ3 contains a methonine (M^{659}) at this position, which is more suitable for hydrophobic contact expected for class II ligand binding (*31*). Interestingly, PTEN requires both canonical and distal interactions to form a complex with par3-PDZ3 (*16*). Consistent with this claim, our laboratory failed to detect any interaction between par3-PDZ3 and a rhodamine-labeled PTEN peptide $QHSQITKV_{COO-}$. par3-PDZ3 is reported to bind a longer PTEN peptide $DEDQHSQITKV_{COO-}$ with a K_d of 19 μM (*16*), which corresponds to a free energy of approximately −6 kcal/mol. Assuming conservatively that 3 kcal/mol of stabilization is derived from distal hydrogen bonding [1 kcal/mol for each hydrogen bond from the DED motif (Figure 5B)], the remaining energy would be extracted from classical PDZ binding of the C-terminal tail. However, this translates into a C-terminal binding affinity of only ~6 mM, which may explain the lack of detectable interaction observed for the short PTEN peptide. In contrast, a short C-terminal VE-Cad peptide $QEELII_{COO-}$ binds par3-PDZ3 with an affinity of 28 μM (Figure 3A). This is likely

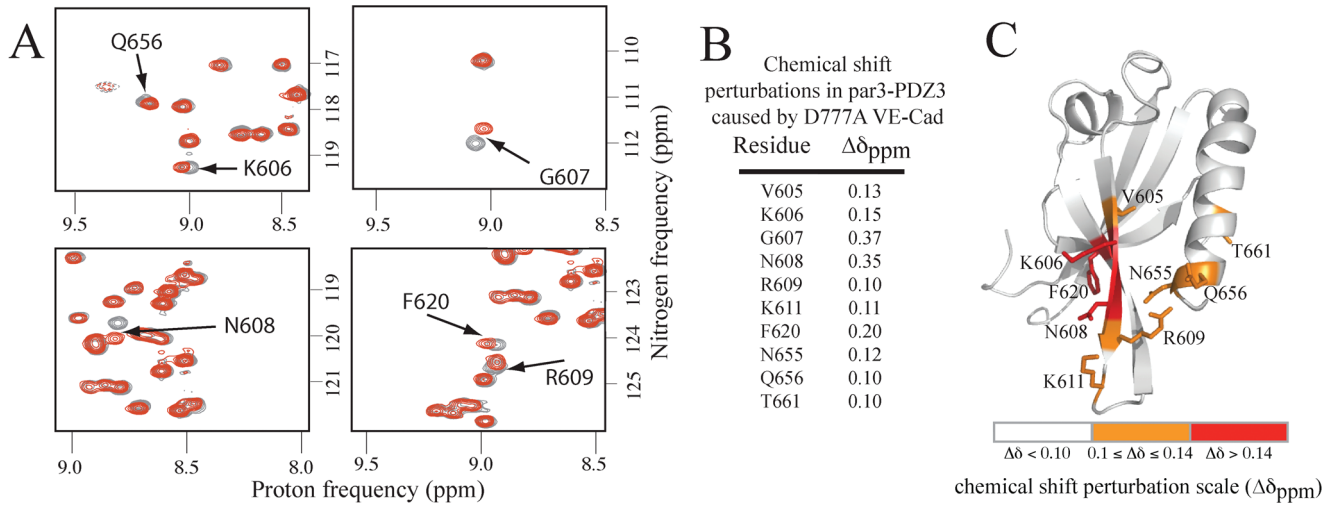

FIGURE 4: (A) Highlighted regions of $^{15}N-^{1}H$ HSQC spectra of the par3-PDZ3 saturated with VE-Cad peptide (MLAELYGSDPQEELII$_{COO-}$) colored gray, overlaid with spectra of the saturated mutant VE-Cad peptide [MLAELYGS(A)PQEELII$_{COO-}$] colored red. (B) Chemical shift difference in par3-PDZ3 calculated from the relationship $\Delta\delta_{ppm} = [(5\Delta\delta_{HN})^2 + (\Delta\delta_N)^2]^{1/2}$, where $\Delta\delta_{HN}$ and $\Delta\delta_N$ represent chemical shift differences between the two saturated forms of par3-PDZ3. All residues with a $\Delta\delta_{ppm}$ of > 0.09 are shown. (C) par3-PDZ3 chemical shift map resulting from D777A binding relative to wild-type VE-Cad binding. Highlighted residues indicate changes in the electronic environment for a region along strand $\beta 2$ consistent with a disruption of distal contact.

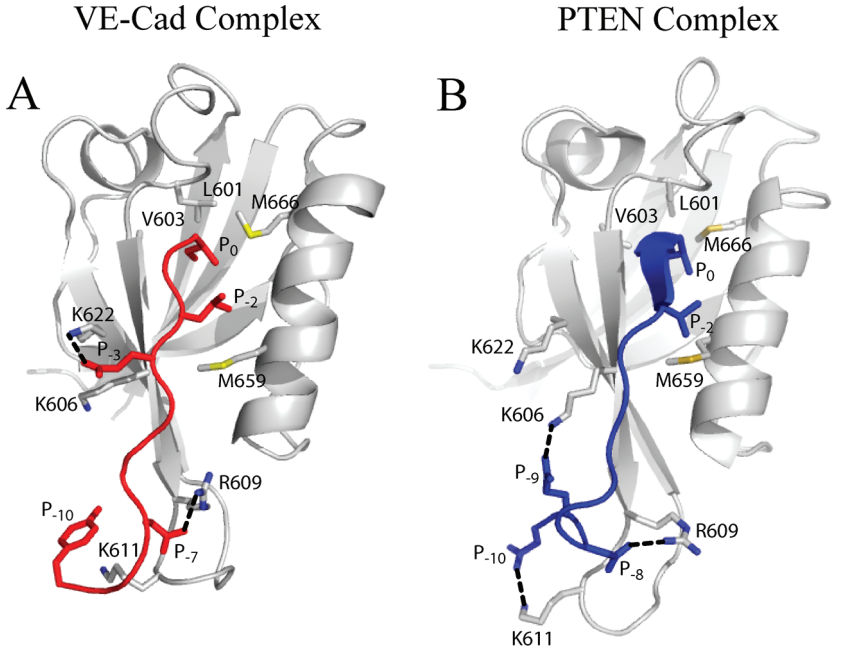

FIGURE 5: (A) Structure of par3-PDZ3 in complex with the C-terminus of VE-Cad. VE-Cad is colored red, with P_n terms denoting amino acid positions within the peptide. Numbered amino acids correspond to side chain locations within par3-PDZ3 involved in peptide binding. Dashed lines show nitrogen−oxygen distances of < 3 Å that indicate areas of probable electrostatic contact. (B) Structure of par3-PDZ3 in complex with the C-terminus of PTEN (*16*). PTEN is colored blue, with P_n terms denoting amino acid positions within the peptide. Numbered amino acids correspond to side chain locations within par3-PDZ3 involved in peptide binding. Dashed lines show nitrogen−oxygen distances of < 3 Å that indicate areas of probable electrostatic contact.

due to favorable hydrophobic contact (figure 2C), and electrostatic contributions betwen P_{-3} (E^{781}) and K^{622} (Figure 5). Considering just canonical C-terminal interactions, VE-Cad QEELII$_{COO-}$ binds par3-PDZ3 ~200 times more strongly than PTEN QHSQITKV$_{COO-}$. As a result, PTEN binding depends on compensatory distal contacts to overcome extremely weak canonical contacts, while VE-Cad binding exploits a complementary interaction surface with distal contacts augmenting PDZ binding. While both ligands employ similar binding modes, there is a difference in the balance between canonical and distal contributions to the free energy of binding. Thus, the unique molecular architecture of par3-PDZ3 allows dual class specificity by providing an additional interaction surface outside the canonical binding pocket that can be optimized to overcome deficiencies resulting from noncomplementary ligand class interactions.

Summary. We characterized the canonical PDZ binding expected for a class II C-terminal ligand involving the P_0 and P_{-2} register of VE-Cad. Our NMR data also revealed evidence of distal contacts outside the canonical binding mode involving upstream residues P_{-10} and P_{-7} of VE-Cad and a patch of basic residues in par3-PDZ3. We inferred from structural results that

the acidic side chain of D^{777} in VE-Cad pairs with R^{609} in strand β2 of par3-PDZ3 to enhance binding through favorable electrostatic interaction. This distal pairing was further confirmed by fluorescence polarization, which demonstrated a decrease in binding affinity upon mutation of either residue. This work provides a detailed view of par3−VE-Cad binding and clarifies the role distal binding modes play in ligand specificity associated with PDZ domain-based protein−protein interactions.

ACKNOWLEDGMENT

We thank Professor Ken Prehoda at the University of Oregon (Eugene, OR) for graciously donating murine par3 DNA. R.C.T. thanks Davin Jensen for technical support.

SUPPORTING INFORMATION AVAILABLE

MALDI-MS and NMR verification of a doubly labeled VE-Cad peptide and a diagram depicting all intermolecular NOE contacts. This material is available free of charge via the Internet at http://pubs.acs.org.

REFERENCES

1. Ceol, A., Chatr-aryamontri, A., Santonico, E., Sacco, R., Castagnoli, L., and Cesareni, G. (2007) DOMINO: A database of domain-peptide interactions. *Nucleic Acids Res. 35*, D557–D560.
2. Castagnoli, L., Costantini, A., Dall'Armi, C., Gonfloni, S., Montecchi-Palazzi, L., Panni, S., Paoluzi, S., Santonico, E., and Cesareni, G. (2004) Selectivity and promiscuity in the interaction network mediated by protein recognition modules. *FEBS Lett. 567*, 74–79.
3. Kennedy, M. B. (1995) Origin of PDZ (DHR, GLGF) domains. *Trends Biochem. Sci. 20*, 350.
4. Hillier, B. J., Christopherson, K. S., Prehoda, K. E., Bredt, D. S., and Lim, W. A. (1999) Unexpected modes of PDZ domain scaffolding revealed by structure of nNOS-syntrophin complex. *Science 284*, 812–815.
5. Penkert, R. R., DiVittorio, H. M., and Prehoda, K. E. (2004) Internal recognition through PDZ domain plasticity in the Par-6-Pals1 complex. *Nat. Struct. Mol. Biol. 11*, 1122–1127.
6. Zimmermann, P., Meerschaert, K., Reekmans, G., Leenaerts, I., Small, J. V., Vandekerckhove, J., David, G., and Gettemans, J. (2002) PIP(2)-PDZ domain binding controls the association of syntenin with the plasma membrane. *Mol. Cell 9*, 1215–1225.
7. Jelen, F., Oleksy, A., Smietana, K., and Otlewski, J. (2003) PDZ domains: Common players in the cell signaling. *Acta Biochim. Pol. 50*, 985–1017.
8. Doyle, D. A., Lee, A., Lewis, J., Kim, E., Sheng, M., and MacKinnon, R. (1996) Crystal structures of a complexed and peptide-free membrane protein-binding domain: Molecular basis of peptide recognition by PDZ. *Cell 85*, 1067–1076.
9. Vaccaro, P., and Dente, L. (2002) PDZ domains: Troubles in classification. *FEBS Lett. 512*, 345–349.
10. Borg, J. P., Marchetto, S., Le Bivic, A., Ollendorff, V., Jaulin-Bastard, F., Saito, H., Fournier, E., Adelaide, J., Margolis, B., and Birnbaum, D. (2000) ERBIN: aA basolateral PDZ protein that interacts with the mammalian ERBB2/HER2 receptor. *Nat. Cell Biol. 2*, 407–414.
11. Kurschner, C., Mermelstein, P. G., Holden, W. T., and Surmeier, D. J. (1998) CIPP, a novel multivalent PDZ domain protein, selectively interacts with Kir4.0 family members, NMDA receptor subunits, neurexins, and neuroligins. *Mol. Cell. Neurosci. 11*, 161–172.
12. Kang, B. S., Cooper, D. R., Devedjiev, Y., Derewenda, U., and Derewenda, Z. S. (2003) Molecular roots of degenerate specificity in syntenin's PDZ2 domain: Reassessment of the PDZ recognition paradigm. *Structure 11*, 845–853.
13. Songyang, Z., Fanning, A. S., Fu, C., Xu, J., Marfatia, S. M., Chishti, A. H., Crompton, A., Chan, A. C., Anderson, J. M., and Cantley, L. C. (1997) Recognition of unique carboxyl-terminal motifs by distinct PDZ domains. *Science 275*, 73–77.
14. Kozlov, G., Banville, D., Gehring, K., and Ekiel, I. (2002) Solution structure of the PDZ2 domain from cytosolic human phosphatase hPTP1E complexed with a peptide reveals contribution of the β2-β3 loop to PDZ domain-ligand interactions. *J. Mol. Biol. 320*, 813–820.
15. Birrane, G., Chung, J., and Ladias, J. A. (2003) Novel mode of ligand recognition by the Erbin PDZ domain. *J. Biol. Chem. 278*, 1399–1402.
16. Feng, W., Wu, H., Chan, L. N., and Zhang, M. (2008) Par-3-mediated junctional localization of the lipid phosphatase PTEN is required for cell polarity establishment. *J. Biol. Chem. 283*, 23440–23449.
17. Ebnet, K., Suzuki, A., Horikoshi, Y., Hirose, T., Meyer Zu Brickwedde, M. K., Ohno, S., and Vestweber, D. (2001) The cell polarity protein ASIP/PAR-3 directly associates with junctional adhesion molecule (JAM). *EMBO J. 20*, 3738–3748.
18. Takekuni, K., Ikeda, W., Fujito, T., Morimoto, K., Takeuchi, M., Monden, M., and Takai, Y. (2003) Direct binding of cell polarity protein PAR-3 to cell-cell adhesion molecule nectin at neuroepithelial cells of developing mouse. *J. Biol. Chem. 278*, 5497–5500.
19. Cai, Y., Stafford, L. J., Bryan, B. A., Mitchell, D., and Liu, M. (2005) G-protein-activated phospholipase C-β, new partners for cell polarity proteins Par3 and Par6. *Oncogene 24*, 4293–4300.
20. Wu, H., Feng, W., Chen, J., Chan, L. N., Huang, S., and Zhang, M. (2007) PDZ domains of Par-3 as potential phosphoinositide signaling integrators. *Mol. Cell 28*, 886–898.
21. Ebnet, K., Aurrand-Lions, M., Kuhn, A., Kiefer, F., Butz, S., Zander, K., Meyer zu Brickwedde, M. K., Suzuki, A., Imhof, B. A., and Vestweber, D. (2003) The junctional adhesion molecule (JAM) family members JAM-2 and JAM-3 associate with the cell polarity protein PAR-3: A possible role for JAMs in endothelial cell polarity. *J. Cell Sci. 116*, 3879–3891.
22. Iden, S., Rehder, D., August, B., Suzuki, A., Wolburg-Buchholz, K., Wolburg, H., Ohno, S., Behrens, J., Vestweber, D., and Ebnet, K. (2006) A distinct PAR complex associates physically with VE-cadherin in vertebrate endothelial cells. *EMBO Rep. 7*, 1239–1246.
23. Delaglio, F., Grzesiek, S., Vuister, G. W., Zhu, G., Pfeifer, J., and Bax, A. (1995) NMRPipe: A multidimensional spectral processing system based on UNIX pipes. *J. Biomol. NMR 6*, 277–293.
24. Bartels, C., Xia, T., Billeter, M., Güntert, P., and Wüthrich, K. (1995) The program XEASY for Computer-Supported NMR Spectral Analysis of Biological Molecules. *J. Biomol. NMR 6*, 277–293.
25. Stuart, A. C., Borzilleri, K. A., Withka, J. M., and Palmer, A. G., III (1999) Compensating for Variations in ^{1}H-^{13}C Scalar Coupling Constants in Isotope-Filtered NMR experiments. *J. Am. Chem. Soc. 121*, 5346–5347.
26. Cornilescu, G., Delaglio, F., and Bax, A. (1999) Protein backbone angle restraints from searching a database for chemical shift and sequence homology. *J. Biomol. NMR 13*, 289–302.
27. Guntert, P. (2004) Automated NMR structure calculation with CYANA. *Methods Mol. Biol. 278*, 353–378.
28. Linge, J. P., Williams, M. A., Spronk, C. A., Bonvin, A. M., and Nilges, M. (2003) Refinement of protein structures in explicit solvent. *Proteins 50*, 496–506.
29. Schwieters, C. D., Kuszewski, J. J., Tjandra, N., and Clore, G. M. (2003) The Xplor-NIH NMR molecular structure determination package. *J. Magn. Reson. 160*, 65–73.
30. Blom, N., Sicheritz-Ponten, T., Gupta, R., Gammeltoft, S., and Brunak, S. (2004) Prediction of post-translational glycosylation and phosphorylation of proteins from the amino acid sequence. *Proteomics 4*, 1633–1649.
31. Bezprozvanny, I., and Maximov, A. (2001) Classification of PDZ domains. *FEBS Lett. 509*, 457–462.